ARTICLES

Structures and Stabilities of Pb_n ($n \leq 20$) Clusters

Xiao-Ping Li,[†] Wen-Cai Lu,*[,†,‡] Qing-Jun Zang,[§] Guang-Ju Chen,[§] C. Z. Wang,[||] and K. M. Ho[||]

State Key Laboratory of Theoretical and Computational Chemistry, Institute of Theoretical Chemistry, Jilin University, Changchun 130021, P. R. China, Laboratory of Fiber Materials and Modern Textile, the Growing Base for State Key Laboratory and College of Physics, Qingdao University, Qingdao 266071, P. R. China, College of Chemistry, Beijing Normal University, Beijing 100875, P. R. China, and Ames Laboratory, U.S. DOE and Department of Physics and Astronomy, Iowa State University, Ames, Iowa 50011

Received: November 17, 2008; Revised Manuscript Received: April 9, 2009

We have performed global structural optimizations for neutral lead clusters Pb_n ($n = 2-20$) by using a genetic algorithm (GA) coupled with a tight-binding (TB) potential. The low-energy structures identified from a GA/TB search were further optimized at the DFT-PBE level. The calculated results show that the Pb_n ($14 < n \leq 20$) clusters favor compact spherical structures with hexagon and pentagon rings. These structures are different from those of Si_n, Ge_n, and Sn_n clusters which favor prolates in the same size range. The binding energies, second differences in energy, and fragmentation behaviors of the Pb_n clusters were also discussed. Pb_n ($n = 4$, 7, 10, 13, 15, and 17) clusters are found to be special stable clusters, which is in good agreement with the experimental results.

I. Introduction

Cluster research is primarily driven by the interest in the evolution of the structures and properties of materials from molecular to macroscopic systems. Clusters with novel properties, such as enhanced stabilities, tunable gaps, and magnetic properties, can lead to novel materials. During the past decades, the structures and physicochemical properties of the clusters of group-IV elements[1−18] have been the subjects of intense research because of the fundamental interest in understanding their bonds and growth patterns and the possibilities of applications in nanotechnology; it is important to elucidate the transition from microscopic molecular state to macroscopic solid system. The group-IV elements exhibit different bonding characters from C to Pb. Compared to the extensive studies and comprehensive understanding of the structures and properties of other group-IV clusters such as carbon,[1−3] silicon,[5,6,9] germanium,[7,11,14] and tin[16,17] clusters, the knowledge about heavier lead clusters is very limited. It has been shown that small Si_n, Ge_n, and Sn_n clusters favor prolate structures, and the structural transitions from prolates to compact near-spherical structures occur in different ranges, around $n = 24-34$ for Si_n,[18−20] $n = 65-74$ for Ge_n,[21] and $n = 35-65$ for Sn_n.[17] In contrast, the Pb_n clusters in the range 11−20 prefer compact structures[22−27] other than prolates because of their metallic bonding property and also relativistic effect.

Experimental studies[28−37]on lead clusters so far include the measurements of dissociation energies, mass spectra, ionization potentials, photoelectron spectroscopy, electron affinities, and chemical reactivity. Theoretically, Lai et al.[38] studied the structures of Pb_n clusters in the size range of $3 < n < 56$ by using the n-body Gupta potential to account for the interactions between the atoms in clusters. Wang et al.[26] studied the Pb_n ($n = 2-22$) clusters by using the DMol package with the BLYP functional. Rajesh et al.[27] investigated the stable structures of Pb_n ($n = 2-15$) with DFT method under the generalized gradient approximation (GGA). From these previous studies, the structures and some properties of Pb clusters in the size range of 2−15 have been determined; however, the larger Pb clusters and the comparison among Si, Ge, Sn, and Pb clusters are not well known.

In this work, we used a genetic algorithm (GA) coupled with a tight-binding (TB) potential to search for ground-state structures of Pb_n clusters ($n = 2-20$). Then, we optimized the low-energy candidates from a GA/TB search at the DFT-PBE level. The lowest-energy structures of Pb_n clusters with $n = 2-13$ obtained from our study agree with those reported previously.[27] For the clusters of $n = 14-20$, we obtained more stable structures than those reported in the literatures[26,27] except for $n = 15$. In addition, binding energies (BEs), second differences in energy, and fragmentation behaviors of Pb_n clusters ($n = 2-20$) were also discussed in details. It is found that Pb_n clusters with $n = 4$, 7, 10, 13, 15, and 17 are special stable clusters, which are in good agreement with the experimental results.[8]

II. Computational Methods

The GA approach has been successfully used in global structural optimizations of cluster structures, for example, medium-sized silicon, germanium, and aluminum clusters.[14,37−41] In this work, we used the GA in combination with a TB potential to search for the low-energy structures of Pb_n clusters. The candidate structures of Pb_n clusters from a GA/TB search were optimized further by using DFT method with project-augmented

* Corresponding author. E-mail: wencailu@jlu.edu.cn.
† Jilin University.
‡ Qingdao University.
§ Beijing Normal University.
|| Iowa State University.

10.1021/jp810107c CCC: $40.75 © 2009 American Chemical Society
Published on Web 05/12/2009

TABLE 1: Relative Energies (in eV) of Pb_{16} Isomers with Respect to That of the Lowest-Energy Isomer Pb_{16}a[a]

	Pb_{16}**a**	Pb_{16}**b**	Pb_{16}**c**	Pb_{16}**d**
E_0	0.00	−0.02	0.08	0.63
E_0^{LS}	0.00	0.04	0.20	0.45
E^{LS}	0.00	0.04	0.20	0.43

[a] E_0 are the DFT-PBE relative energies without the spin−orbit effects; E_0^{LS} are the single-point relative energies with the spin−orbit effects, based on the geometries optimized at DFT-PBE without the spin−orbit effects; and E^{LS} are the relative energies resulted from the DFT-PBE optimizations with the spin−orbit effects.

wave (PAW) and Perdew−Burke−Ernzerhof (PBE) pseudopotential as implemented in VASP.[42] The PAW-PBE pseudopotential was generated by taking scalar relativistic corrections into account, and the exchange-correlation energy was calculated by the PBE functional. The cutoff of plane wave in the VASP calculations is taken to be 98.0 eV. The geometry optimization of each isomer is carried out until the energy is converged to an accuracy of 10^{-5} eV.

Balasubramanian et al.[34,36] have carried out a series of studies on small Pb clusters and found that the effect of spin−orbit coupling is important for small Pb clusters. For the Pb_{16-20} isomers, the energy orders with the spin−orbit coupling effects are found to be the same as those without the spin−orbit effects except for Pb_{16}. As shown in Table 1, the single-point relative energies (E_0^{LS}) corrected by the spin−orbit coupling effects are very close to those (E^{LS}) from the optimizations with the spin−orbit effects. Thus, in this work, we just performed the single-point energy calculations with the spin−orbit coupling effects.

In order to search for low-energy Pb_n structures, a large number of initial geometries based on tetragonal, pentagonal, or hexagonal growth motifs and those reported for Si, Ge, Sn, and Pb clusters had been considered. Structures of Pb_n formed by adding or removing one or two atoms on the basis of the low-energy neighbor structures (Pb_{n-1}, Pb_{n-2}, Pb_{n+1}, and Pb_{n+2}) were also considered.

III. Results and Discussion

A. Geometries. The lowest-energy structures and some representative isomers of neutral Pb_n ($n = 2-15$) and Pb_n ($n = 16-20$) clusters are shown in Figures 1 and 2. The stable structures of Pb_n clusters ($n = 2-15$) agree well with those previously reported except for Pb_{14}.[27] The Pb clusters with $n \leqslant 7$ have structures similar to those of Si, Ge, and Sn clusters. Pb_8 and Pb_9 are formed by adding one or two atoms to the Pb_7 structure. The lowest-energy structure of Pb_{10} is a capped trigonal prism, similar to Si_{10}, Ge_{10}, and Sn_{10}; Pb_{13} favors an encapsulated icosahedron structure, as shown in Figure 1. The most stable isomers of Pb_{12} (C_{5v}) and Pb_{11} (C_{2v}) can be obtained from the icosahedron structure of Pb_{13} by moving away one central atom of Pb_{13}**a** to get Pb_{12} and further removing another atom at the bottom of Pb_{12} to get Pb_{11}, which are different from Si_n, Ge_n, and Sn_n ($n = 11$ and 12) clusters.

For Pb_{14} clusters, the reported lowest-energy isomer of Pb_{14}**b** (Figure 1) was a structure with an atom capped on Pb_{13}**a**.[27] However, we found that the structure Pb_{14} **a** (Figure 1) is about 0.01 eV lower in energy than that of Pb_{14}**b**. The structure of Pb_{14}**a** can be regarded as a Pb_{10}**b** and a Pb_5 gathering with one common vertex atom. Pb_{15}**a** is an encapsulated hexagonal structure, consistent with that of the previous studies.[26,27] Pb_{15}**b** is a distorted structure compared with Pb_{15}**a**; Pb_{15}**c** is formed by adding one atom at the center of Pb_{14}**a**, and Pb_{15}**d** is a 1−5−3−5−1 layer-stacking structure.

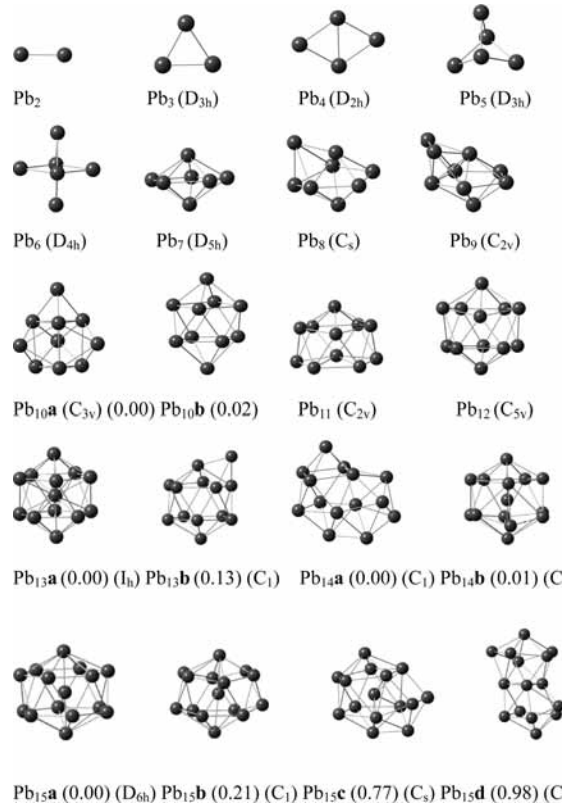

Figure 1. Lowest-energy structures of Pb_n ($n = 2-15$) calculated at the DFT-PBE level. Values (in eV) in brackets are the relative energies with the spin−orbit effects with respect to the lowest-energy isomer.

For Pb_{16} cluster, the lowest-energy structure Pb_{16}**a** is composed of two Pb_6 caps linked by a Pb_4 ring, leading to a 1−5−4−5−1 layer staking. Compared to Pb_{16}**a**, the energies of the other three isomers **b**, **c**, and **d** are 0.04, 0.20, and 0.45 eV higher, respectively. Pb_{16}**b** can be considered to be formed by capping one atom on the bottom of Pb_{15}**a**.

For Pb_{17} cluster, the lowest-energy structure Pb_{17}**a** has C_{2v} symmetry. It can be considered as a perfect cage. The second lowest-energy structure is 1−5−5−5−1 stacked (Figure 2). The difference between Pb_{17}**c** and Pb_{17}**d** is that the added atom locates at the different locations (bottom and side surface, respectively) of Pb_{16}**b**.

For Pb_{18} cluster, the most stable structure Pb_{18}**a** favors a 1−6−1−6−3−1 stacking cage structure with C_{3v} symmetry. It can be obtained by adding one atom on the trigonal bottom of Pb_{17}**c**. Pb_{18}**b** and Pb_{18}**c** are related to Pb_{17}**a** and Pb_{17}**b**, respectively. Pb_{18}**b** exhibits C_{2v} symmetry and is 0.08 eV less stable than Pb_{18}**a**. Pb_{18}**c** with D_{5h} symmetry consists of three stacking pentagons, and there is one atom at the center of the middle pentagon. Pb_{18}**d** can be considered to have one more atom added on the side surface of Pb_{17}**c**.

The most stable isomer Pb_{19}**a** is formed by attaching one atom at the central layer of Pb_{18}**c,** leading to a hexagon, which is a cage structure with C_2 symmetry. Pb_{19}**b** (C_1) is formed by a gathering of Pb_9 and Pb_{10}. Pb_{19}**c** is has a pattern similar to that of Pb_{17}**a**. Pb_{19}**d**, as shown in Figure 2, is a well-known double icosahedron with a 1−5−1−5−1−5−1 stacking. However, this structure is not energetically favorable for Pb_{19}.

The lowest-energy isomer Pb_{20}**a** has D_{2h} symmetry, which can be considered to be composed of two Pb_7s linked by a

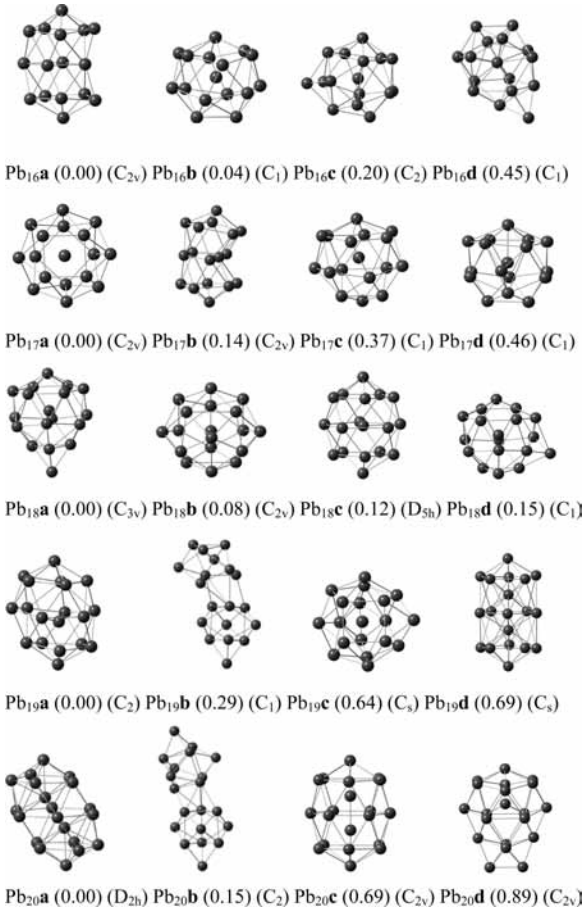

Figure 2. Low-lying isomers of Pb_n ($n = 16-20$) calculated at the DFT-PBE level. Values (in eV) in brackets are the relative energies with the spin−orbit effects with respect to the lowest-energy isomer.

hexagon. Pb_{20}**b** (C_2), composed of two Pb_{10}**s**, is 0.15 eV less stable than Pb_{20}**a**. Pb_{20}**c** (C_{2v}) is an up-and-down symmetrical stacking of two Pb_7s linked by a hexagon.

From Si down to Pb in group-IV elements, the covalent bonding property is getting weaker, and the metallic property becomes stronger. Thus, the clusters of Si, Ge, Sn, and Pb may exhibit different structure motifs. For small Si_n, Ge_n, Sn_n, and Pb_n clusters with $n = 4$, 7, and 10, they have similar geometries. In the size range of 16−20, the structures of Si, Ge, and Sn clusters favor prolate geometries, but Pb clusters prefer compact near-spherical structures. Sn and Pb are closest-neighbor elements in the periodic table; thus, they may be expected to have some common properties. However, the calculated results show that the Sn_n clusters in the size range of 17−20 consist of bunching Sn_{10} units,[16] but near-spherical compact structures are dominant for the Pb_n clusters in this range.

Although the structures of Pb and Al clusters choose the compact spherical shapes, they are different in details in the range of $n = 14-20$.[39,41] For example, Al_{14}, Al_{15}, and Al_{16} are constructed on the basis of the ideal icosahedron structure of Al_{13}, with one, two, or three more atoms attached on it, respectively. However, Pb_{14}**a** is formed by a combination of a Pb_5 and a Pb_{10}**b** with one common atom; Pb_{15}**a** is an encapsulated hexagonal structure, and Pb_{16}**a** is a 1−5−4−5−1 staking structure. The lowest-energy structure of Al_{17} is constructed by capping four atoms on an icosahedron with two sets of two adjacent atoms located on opposite symmetric positions of the icosahedron. Pb_{17}**a** is found to be a special symmetrical cage, which does not appear in previous studies of Al clusters. Al_{18} is formed by capping one more atom to the stable Al_{17}, Al_{19} is a structure with five adjacent atoms and an individually atom capping on a decahedron, and Al_{20} has one more atom embedded in the double icosahedrons isomer of Al_{19}. However, Pb_{18}**a** with C_{3v} symmetry favors a 1−6−1−6−3−1 stacking pattern; Pb_{19}**a** can be considered to be constructed on the basis of an icosahedron, by moving one core atom to surface; and Pb_{20}**a** consists of two Pb_7s linked by a hexagon.

We also calculated the ratios of clusters' BEs per atom (E_b) over the corresponding BE of bulk (E_b^0) for Si, Ge, Sn, Pb, and Al. The results are given in Table 2. For these five kinds of clusters, the E_b/E_b^0 ratios of small Al_n ($n = 4$, 7, 10, 13, and 20) clusters are the smallest, those of Sn_n ($n = 7$, 10, 13, and 20) clusters are the largest, and those of Ge_n and Pb_n ($n = 7$, 10, 13, and 20) clusters are only slightly smaller compared to those of the corresponding Sn_n clusters. Thus, small Ge, Sn, and Pb clusters are more stable compared to small Al clusters, consistent with the results of theoretical predictions that medium Si, Ge, and Sn clusters favor the structures composed by bunch gathering of small stable clusters. Similarly, the Pb clusters in the medium-sized range with structures stacked by small stable clusters can be expected to be favored.

B. Stabilities. In order to understand the relative stabilities of Pb_n clusters, we have calculated BEs, second differences in energy, and fragmentation behaviors based on the total energies of the lowest-energy structures.

The BE per atom of Pb_n cluster is defined by $BE = [nE(Pb) - E(Pb_n)]/n$, in which $E(Pb_n)$ and $E(Pb)$ are the energies of a Pb_n cluster and a free Pb atom, respectively. It is clear from Table 3 and Figure 3 that the BEs per atom of the ground-state Pb_n clusters increase rapidly with the cluster size up to $n = 8$, and the curve becomes smoother in the size range of 9−20. Small humps in the BE curve indicate large stability for some specific clusters. In particular, at Pb_7, Pb_{10}, Pb_{15}, and Pb_{17}, there are prominent peaks, showing that these clusters have special stabilities compared with their neighbors.

We can also estimate relative stabilities of the clusters by calculating the second differences in energy, which is defined by $\Delta^2E = [E(Pb_{n+1}) + E(Pb_{n-1}) - 2E(Pb_n)]$. From this expression, clusters which have positive values of Δ^2E are more stable than their neighbors. The Δ^2E curve for Pb_n ($n = 2-19$) clusters is displayed in Figure 4. Pb_n clusters with $n = 4$, 7, 10, 13, 15, and 17 are found to be more stable than their nearest neighbors. This result is in good agreement with previous

TABLE 2: Ratios of BEs per Atom (E_b) of Clusters over Corresponding BEs of Bulk (E_b^0) Calculated at the DFT-PBE Level with the Spin−Orbit Effects

cluster	$E_b(Si_n)/E_b^0$ (diamond-Si)	$E_b(Ge_n)/E_b^0$ (diamond-Ge)	$E_b(Sn_n)/E_b^0$ (diamond-Sn)	$E_b(Pb_n)/E_b^0$ (fcc-Pb)	$E_b(Al_n)/E_b^0$ (fcc-Al)
4	0.69	0.73	0.72	0.67	0.47
7	0.81	0.87	0.88	0.84	0.66
10	0.84	0.89	0.90	0.87	0.69
13	0.82	0.88	0.89	0.88	0.76
20	0.85	0.90	0.91	0.88	0.79

TABLE 3: BEs (E_b) per Atom, Most Favorable Fragmentation Channels, and Fragmentation Energies (E_f) of Pb_n ($n = 2-20$) Clusters Calculated at the DFT-PBE Level with the Spin−Orbit Effects

	BE (eV/atom)	fragmentation channel	E_f (eV)
Pb_2	0.69	$Pb_1 + Pb_1$	1.38
Pb_3	1.09	$Pb_1 + Pb_2$	1.88
Pb_4	1.36	$Pb_1 + Pb_3$	2.19
Pb_5	1.34	$Pb_1 + Pb_4$	1.24
Pb_6	1.59	$Pb_4 + Pb_2$	2.69
Pb_7	1.71	$Pb_1 + Pb_6$	2.44
Pb_8	1.67	$Pb_1 + Pb_7$	1.40
Pb_9	1.74	$Pb_1 + Pb_8$	2.30
Pb_{10}	1.75	$Pb_1 + Pb_9$	1.99
Pb_{11}	1.75	$Pb_1 + Pb_{10}$	1.59
Pb_{12}	1.77	$Pb_1 + Pb_{11}$	2.00
Pb_{13}	1.79	$Pb_7 + Pb_6$	1.82
Pb_{14}	1.76	$Pb_7 + Pb_7$	0.69
Pb_{15}	1.80	$Pb_7 + Pb_8$	1.74
Pb_{16}	1.80	$Pb_7 + Pb_9$	1.14
Pb_{17}	1.81	$Pb_7 + Pb_{10}$	1.08
Pb_{18}	1.78	$Pb_9 + Pb_9$	0.74
Pb_{19}	1.79	$Pb_{10} + Pb_9$	0.78
Pb_{20}	1.80	$Pb_{10} + Pb_{10}$	0.71

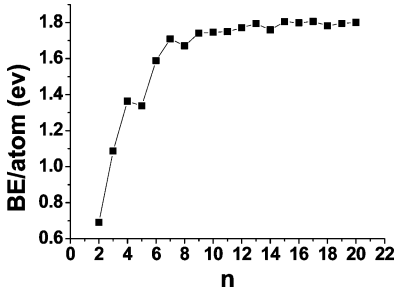

Figure 3. BEs per atom of Pb_n ($n = 2-20$) at the DFT-PBE level with the spin−orbit effects.

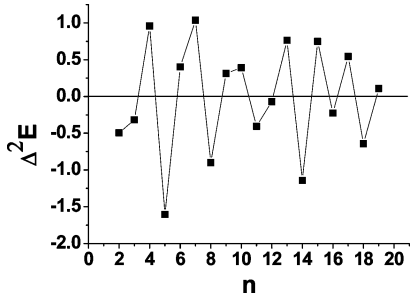

Figure 4. Second differences in energy (in eV), defined by $\Delta^2E = [E(Pb_{n+1}) + E(Pb_{n-1}) - 2E(Pb_n)]$, of Pb_n ($n = 2-20$) calculated at the DFT-PBE level with the spin−orbit effects.

experimental observations.[30] It should be noted that $n = 4$, 7, and 10 are also the magic sizes for Si and Ge clusters.[10]

We have also analyzed the fragmentation behaviors of the Pb_n ($n = 2-20$) clusters. It is known that the fragmentation processes may have dissociation barriers and may be affected by temperature because of entropy contribution. In the present work, we have assumed that the fragmentation pathways are determined only by the total energies of the reactants and products. The fragmentation energy (E_f) is defined by the energy difference between the reactant and its fragmentation products; that is, $E_f = E(Pb_m) + E(Pb_{n-m}) - E(Pb_n)$ with $m < n$. We have calculated all possible fragmentation channels, but we only discuss the easiest ones in the following paragraphs.

The fragmentation energy for the most favorable channel as a criterion of cluster is shown in Figure 5 and is also listed in Table 3. It shows that although small clusters Pb_n ($n \leq 12$) favor a monomer evaporation as the lowest-energy fragmentation channel, larger clusters ($n \geq 13$) prefer to dissociate into two small stable clusters as shown as in Figure 5. Duncan et al.[30] in their photo-ionization experiment have noticed that $n = 14$ is missing in the mass spectrum, and in contrast, Pb_7 is found to be more abundant in mass-spectrometry experiment. According to our fragmentation calculations, Pb_7 is one of the favorable daughter cluster for several fragmentation processes, such as $Pb_{13} \rightarrow (Pb_6 + Pb_7)$, $Pb_{14} \rightarrow (Pb_7 + Pb_7)$, $Pb_{15} \rightarrow (Pb_7 + Pb_8)$, $Pb_{16} \rightarrow (Pb_7 + Pb_9)$, and $Pb_{17} \rightarrow (Pb_7 + Pb_{10})$. The fragmentation energy in the process in which the Pb_{14} cluster dissociates into two Pb_7 daughter clusters is only 0.69 eV; this indicates that such a dissociation into two Pb_7 clusters is easy to occur and can explain the missing Pb_{14} in the photo-ionization experiment.

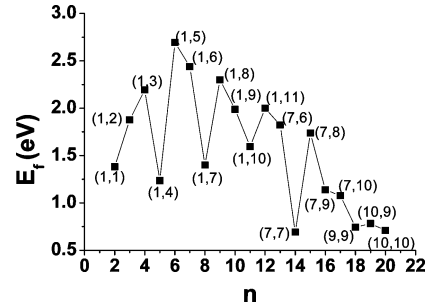

Figure 5. Fragmentation energies (E_f) of the lowest-energy fragmentation channels of Pb_n ($n = 2-20$) calculated at the DFT-PBE level with the spin−orbit effects.

For the clusters with $n > 15$, Pb_{10} emerges as an important daughter cluster in the fragmentation products, for example, $Pb_{17} \rightarrow (Pb_{10} + Pb_7)$, $Pb_{19} \rightarrow (Pb_{10} + Pb_9)$, and $Pb_{20} \rightarrow (Pb_{10} + Pb_{10})$. Therefore, Pb_{10} can be expected to be a special stable cluster. We found that the small magic clusters with the sizes of 4, 7, and 10 are the most abundant daughter clusters, and the same complexions are found in the fragmentation products of Si and Ge clusters.

IV. Conclusion

We have studied the Pb_n ($n = 2 - 20$) clusters by using DFT calculations combined with a GA/TB search. On the basis of the reliable structures obtained from our global optimizations, we analyzed the properties of stable lead clusters including binding energies per atom, second differences in energy, and fragmentation behaviors.

The low-energy cluster structures obtained from our studies can be classified as encapsulation stacked motifs. The most stable geometries of Pb_n clusters up to $n = 7$ are similar to the corresponding Si, Ge, and Sn clusters, and the motifs of larger clusters prefer the different patterns from the other Group-IV clusters. The compact spherical structures are favorable for Pb_n cluster even in the size range of 11−20, different from the same-size Si, Ge, and Sn clusters where the prolate structures are most stable. This fact can be attributed to the metallic character and relativistic effect of Pb.

We noted that the thermodynamic stabilities of Pb_n clusters have an oscillation character, where the Pb_n with $n = 4$, 7, 10, 13, 15, and 17 are more stable than their neighbors. In the fragmentation analyses, Pb_4, Pb_7, and Pb_{10} appear more frequently in fragmentation products. We also found that small lead clusters with $n \leq 10$ have larger fragmentation energies, whereas those clusters with $10 < n \leq 20$ have smaller fragmentation energies. These results suggest that lead clusters

with $10 < n \leq 20$ can be easily dissociated into smaller stable lead clusters. The present calculated results and analyses are consistent with the experimental observations.

Acknowledgment. This work was supported by the National Natural Science Foundation of China (20773047, 20473030, and 60028403). Ames Laboratory is operated for the U.S. Department of Energy by Iowa State University under Contract no. DE-AC02-07CH11358. This work was also supported by the Director for Energy Research, Office of Basic Energy Sciences.

References and Notes

(1) Handschuh, H.; Gantefor, G.; Kessler, B.; Bechthold, P. S.; Eberhardt, W. *Phys. Rev. Lett.* **1995**, *74*, 1095.
(2) Jones, R. O.; Seifert, G. *Phys. Rev. Lett.* **1997**, *79*, 443.
(3) Jones, R. O. *J. Chem. Phys.* **1999**, *110*, 5189.
(4) Cui, L. F.; Huang, X.; Wang, L. M.; Li, J.; Wang, L. S. *J. Phys. Chem. A* **2006**, *110*, 10169.
(5) Binggeli, N.; Chelikowsky, J. R. *Phys. Rev. Lett.* **1995**, *75*, 493.
(6) Liu, B.; Lu, Z. Y.; Pan, B.; Wang, C. Z.; Ho, K. M.; Shvartsburg, A. A.; Jarrold, M. F. *J. Chem. Phys.* **1998**, *109*, 9401.
(7) Lu, Z. Y.; Wang, C. Z.; Ho, K. M. *Phys. Rev. B* **2000**, *61*, 2329.
(8) Sattler, K.; Muhlbach, J.; Echt, O.; Pfau, P.; Recknagel, E. *Phys. Rev. Lett.* **1981**, *47*, 160.
(9) Jackson, K. A.; Horoi, M.; Chaudhuri, I.; Frauenheim, T.; Shvartsburg, A. A. *Phys. Rev. Lett.* **2004**, *93*, 013401.
(10) Martin, T. P.; Schaber, H. *J. Chem. Phys.* **1985**, *83*, 855.
(11) Wang, J. L.; Wang, G. H.; Zhao, J. J. *Phys. Rev. B* **2001**, *64*, 205411.
(12) Shvartsburg, A. A.; Jarrold, M. F. *Chem. Phys. Lett.* **2000**, *317*, 615.
(13) Mazzone, A. M. *Phys. Rev. B.* **1996**, *54*, 5970.
(14) Zhao, L. Z.; Lu, W. C.; Qin, W.; Zang, Q. J.; Wang, C. Z.; Ho, K. M. *Chem. Phys. Lett.* **2008**, *455*, 225.
(15) Dai, D.; Balasubramanian, K. *J. Chem. Phys.* **1992**, *96*, 8345.
(16) Majumder, C.; Kumar, V.; Mizuseki, H.; Kawazoe, Y. *Phys. Rev. B* **2001**, *64*, 233405.
(17) Shvartsburg, A. A.; Jarrold, M. F. *Phys. Rev. A* **1999**, *60*, 1235.
(18) Pushpa, R.; Waghmare, U.; Narasimhan, S. *Phys. Rev. B* **2008**, *77*, 045427.
(19) Jarrold, M. F.; Constant, V. A. *Phys. Rev. Lett.* **1991**, *67*, 2994.
(20) Jarrold, M. F.; Bower, J. E. *J. Chem. Phys.* **1992**, *96*, 9180.
(21) Hunter, J. M.; Fye, J. L.; Jarrold, M. F.; Bower, J. E. *Phys. Rev. Lett.* **1994**, *73*, 2063.
(22) Christensen, N. E.; Satpathy, S.; Pawlowska, Z. *Phys. Rev. B* **1986**, *34*, 5977.
(23) Rajesh, C.; Majumder, C. *J. Chem. Phys.* **2007**, *126*, 244704.
(24) Wei, C. M.; Cheng, C.; Chang, C. M. *J. Phys. Chem. B* **2006**, *110*, 24642.
(25) Schafer, S.; Heiles, S.; Becker, J. A.; Schafer, R. *J. Chem. Phys.* **2008**, *129*, 044304.
(26) Wang, B. L.; Zhao, J. J.; Chen, X. S.; Shi, D. N.; Wang, G. H. *Phys. Rev. A* **2005**, *71*, 033201.
(27) Rajesh, C.; Majumder, C.; Rajan, M. G. R.; Kulshreshtha, S. K. *Phys. Rev. B* **2005**, *72*, 235411.
(28) Gingerich, K. A.; Cocke, D. L.; Miller, F. *J. Chem. Phys.* **1976**, *64*, 4027.
(29) Stranz, D. D.; Khanna, R. K. *J. Chem. Phys.* **1981**, *74*, 2116.
(30) Laihing, K.; Wheeler, R. G.; Wilson, W. L.; Duncan, M. A. *J. Chem. Phys.* **1987**, *87*, 3401.
(31) Farley, R. W.; Ziemann, P.; Castleman, A. W., Jr. *Z. Phys. D: At., Mol. Clusters* **1989**, *14*, 353.
(32) Gantefor, G.; Gausa, M.; Meiwes-Broer, K. H.; Lutz, H. O. *Z. Phys. D: At., Mol. Clusters* **1989**, *12*, 405.
(33) Luder, Ch.; Meiwes-Broer, K. H. *Chem. Phys. Lett.* **1998**, *294*, 391.
(34) Balasubramanian, K.; Majumdar, D. *J. Chem. Phys.* **2001**, *115*, 8795.
(35) Farley, R. W.; Ziemann, P.; Keesee, R. G.; Castleman, A. W., Jr. *Z. Phys. D: At., Mol. Clusters* **1989**, *25*, 267.
(36) Zhao, C. Y.; Balasubramanian, K. *J. Chem. Phys.* **2002**, *116*, 10287.
(37) Iniguez, M. P.; Lopez, M. J.; Alonso, J. A.; Soler, J. M. *Z. Phys. D: At., Mol. Clusters* **1989**, *11*, 163.
(38) Lai, S. K.; Hsu, P. J.; Liu, W. K.; Iwamatsu, M. *J. Chem. Phys.* **2002**, *117*, 10176.
(39) Sun, J.; Lu, W. C.; Li, Z. S.; Wang, C. Z.; Ho, K. M. *J. Chem. Phys.* **2008**, *129*, 014707.
(40) Zhang, W.; Lu, W. C.; Sun, J.; Wang, C. Z.; Ho, K. M. *Chem. Phys. Lett.* **2008**, *455*, 232.
(41) Chuang, F. C.; Wang, C. Z.; Ho, K. M. *Phys. Rev. B* **2006**, *73*, 125431.
(42) (a) Vienna ab initio simulation package, Technische Universitat Wien 1999 Kresse, G.; Hafner, J. *Phys. Rev. B* **1993**, *47*, 558. (b) Kresse, G.; Furthmuller, J. *Phys. Rev. B* **1996**, *54*, 11169.

JP810107C